Title

Enhanced Osteogenic Differentiation of hMSCs Using BMP@ZIF-8-Loaded GelMA Nanocomposite Hydrogels with Controlled BMP–2 Release

Journal

ACS Omega, 10(11)

ISSN

2470-1343

Authors

Yuan, Weihao
de Almeida Queiroz Ferreira, Luiza
Khade, Ronit
et al.

Publication Date

2025-03-25

DOI

10.1021/acsomega.4c06577

Peer reviewed

ACS OMEGA

Open Access

http://pubs.acs.org/journal/acsodf

Article

Enhanced Osteogenic Differentiation of hMSCs Using BMP@ZIF-8-Loaded GelMA Nanocomposite Hydrogels with Controlled BMP-2 Release

Weihao Yuan,[§] Luiza de Almeida Queiroz Ferreira,[§] Ronit Khade, Ivana Diniz, Sahar Ansari, and Alireza Moshaverinia*

Cite This: *ACS Omega* 2025, 10, 10826−10834

Read Online

ACCESS | Metrics & More | Article Recommendations | Supporting Information

ABSTRACT: Hydrogels are highly versatile materials with immense potential for tissue engineering and regenerative medicine owing to their biocompatibility, tunable mechanical properties, and ability to mimic the natural extracellular matrix. Their 3D porous structure allows for the encapsulation and delivery of bioactive molecules, making them ideal candidates for drug delivery systems. In tissue repair, particularly for bone regeneration, hydrogels can serve as carriers that release therapeutic agents in a controlled manner, thus enhancing the healing process. Zeolitic Imidazolate Framework-8 (ZIF-8) nanoparticles and recombinant human Bone Morphogenetic Protein (rhBMP-2) molecules were incorporated solely (ZIF@GelMA) or in association (BMP@ZIF@GelMA) into gelatin modified by a methacryloyl hydrogel (GelMA) to investigate its physical and osteogenic properties. Hydrogels were characterized by Scanning Electron Microscopy and rheological tests. We analyzed hydrogel degradation and the BSA release profile of BMP@ZIF@GelMA samples throughout 0, 1, 3, 7, 14, and 28 days. Cell adhesion and bone formation markers were analyzed for hydrogel-encapsulated human dental pulp cells by using immunocytochemistry and molecular analysis. ZIF@GelMA and BMP@ZIF@GelMA exhibited a porous and viscoelastic structure with increased storage modulus when rhBMP2 was present. BSA@ZIF@GelMA showed a balanced degradation rate and a controlled release of BSA. The ZIF@GelMA upregulated the expression of cell adhesion and bone formation genes, and when BMP-2 was introduced, the levels of markers were remarkably elevated. BMP@ZIF@GelMA hydrogel presents several favorable factors to promote cellular adhesion and bone regeneration, thus encouraging further prospects for advanced therapeutic applications in tissue repair.

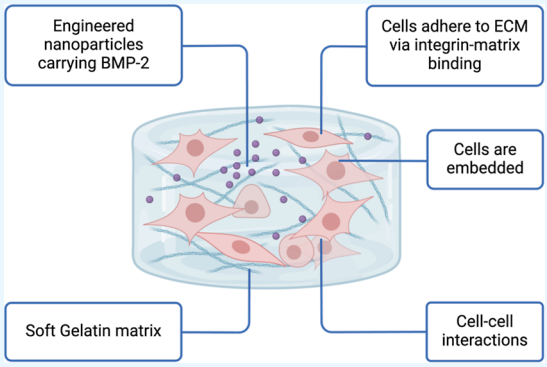

1. INTRODUCTION

Craniofacial bone defects resulting from trauma, cancer, or congenital conditions are a clinical challenge because this tissue may not heal independently.[1−5] Besides lowering the quality of life, it also has a socioeconomic problem, with annual healthcare costs above $600 billion.[6,7] Reconstructive surgeries for repairing bone defects still consist of autograft or allograft techniques.[8,9] The first is considered the gold standard and can be the preferred surgical approach. However, it consists of harvesting tissue from another site, depending on its availability, and the procedure can result in postoperatory complications, increasing pain, susceptibility to pathogen infections, and morbidity of the donor.[10−12] On the other side, allographs are directly affected by the immune response of patients.[13−17] These drawbacks enhanced studies of synthetic substitutes of bone grafts. Certainly, grafts can improve clinical parameters and bone loss progression. However, a major challenge in the bone regeneration field is the limited volume and height of bone neoformation in wider defects.[18−20]

Tissue engineering associated with biological molecules and nanoparticles can help overcome limitations of traditional approaches.[21−23] Synthetic growth factors can lead to functional tissue repair, targeting a clinical application where the damaged tissue is repaired faster.[24−26] Nanofillers or nanoparticles add mechanical strength to a biomaterial, whereas hydrogels may be readily injected into any cavity format.[27−29] Accordingly, hydrogels can mimic the extracellular matrix structure and microenvironment stiffness with sustained release of bioactive molecules, thus supporting cell migration, proliferation, and dedifferentiation followed by tissue regeneration.[30−32] Choosing a particular hydrogel over another is

Received: July 16, 2024
Revised: February 20, 2025
Accepted: February 26, 2025
Published: March 11, 2025

Scheme 1. Schematic Illustration of the Engineered Nanocomposite Hydrogel

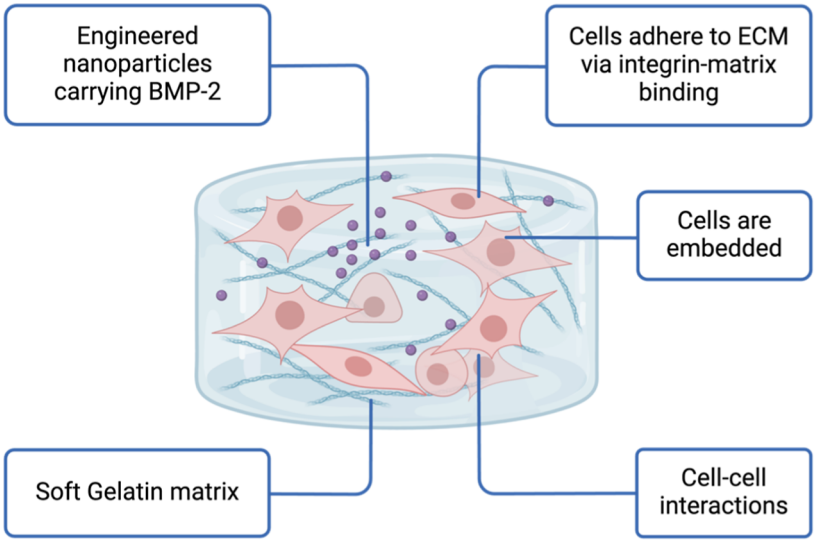

crucial when it comes to targeting injured tissue. For example, conventional hydrogels may not be adherent and may lack mechanical strength or osteogenic properties.[33−35] Conversely, gelatin modified by methacryloyl (GelMA) is bifunctional, and its mechanical properties are suitable for a 3D platform bioprinting using stem-cell-delivering biomaterials or bioactive molecules.[36−40]

Zeolitic Imidazolate Framework-8 (ZIF-8) is considered a Metal−Organic Framework (MOF).[41] It is a type of material containing metallic ions and presenting physical properties such as high porosity, surface area, diverse structure, and unsaturated metal coordination bonds.[42−44] All those characteristics allow modifications or the incorporation of biological molecules to be used as a therapeutic drug, such as an antimicrobial agent.[45,46] Beyond its chemical adaptability, ZIF-8 is recognized for its inherent stability, ensuring it remains unreactive and intact under extreme conditions, such as pH, pressure, and temperature.[44,47] Ultimately, the multifaceted properties of ZIF-8, ranging from its structural adaptability to its medical applications, underscore its potential and importance in scientific research and medical advancements. While several molecules have been studied for bone repair, bone morphogenetic proteins (BMPs) showed potent osteogenic factors.[48−50] Previously, studies have demonstrated that the ZIF-8 and BMP-2 association increased osteogenic properties and dedifferentiation toward bone repair and might be used as a bone graft material.[51−53] The incorporation of these molecules into hydrogels was also reported as a chitosan model. However, a more stable network can be created by adding methacryloyl (GelMA), resulting in better mechanical properties.

Herein, we aimed to develop a GelMA hydrogel system incorporating ZIF-8 nanoparticles and human recombinant bone morphogenetic protein (rhBMP-2) molecules (Scheme 1). We investigated its mechanical and physical properties and assessed its ability to promote short-term cell adhesion and bone differentiation properties.

2. MATERIAL AND METHODS

2.1. Synthesis of the Biomaterial. ZIF-8 nanoparticles (NPs) were synthesized by mixing 2-methyl imidazole (2-MeIM; Sigma-Aldrich, St. Louis, MO, USA) and zinc nitrate (Zn^{2+}; Sigma-Aldrich, St. Louis, MO, USA) in aqueous solution. To get the monodispersed nanoscale ZIF NPs, we optimized the ratio of 2-MeIM and Zn^{2+} to 70:1 at 3150 and 45 mM concentrations, respectively. rhBMP2 (Thermo Fisher Scientific, Waltham, MA, USA) was added at 100 μg/mL concentration during the synthesis of BMP@ZIF NPs. The obtained ZIF NPs and BMP@ZIF NPs were collected by centrifugation at 10,000 g for 5 min and washed three times in phosphate-buffered saline (PBS). The obtained ZIF NPs and BMP@ZIF NPs were mixed with GelMA solution with 0.05% photoinitiator (LAP), followed by UV curation for 15 min.

2.2. Scanning Electron Microscopy. For scanning electron microscopy (SEM) analysis, the samples were flash-frozen by liquid nitrogen and dehydrated under lyophilization for 3 days. Small hydrogel pieces were sputtered with a thin layer of gold (15 mA for 60 s). Image acquisition was performed by using a Zeiss VP40 scanning electron microscope (Zeiss, Mannheim, Germany).

2.3. Rheological Analysis. The rheological analysis and the compressive strength of the samples were conducted in Anton Paar equipment (Graz, Australia) with the following settings: frequency sweep range from 0.01 to 10 Hz; strain sweep from 0.1% to 1000%. Optical measurements were conducted at a 0.5 mm distance between the rotor and the plate.

2.4. Degradation of the Material. The samples previously prepared (n = 6) were immersed in PBS containing 0.1% (w/v) sodium azide (NaN_3) (Sigma−Aldrich). After cautiously removing hydrogels from the solution, the samples were rinsed three times with deionized water, eliminating salt adhesive. Then, samples were kept for 5 min under liquid nitrogen and freeze-dried for 3 days. The dry mass of each sample was assessed at 0, 1, 3, 7, 14, and 28 days, and the weight loss percentage was calculated with the following equation

$$\text{Weight percentage (\%) at day t} = \frac{\text{dry mass on day t}}{\text{dry mass on day 0}} \times 100\%$$

2.5. Bovine Serum Albumin Release. A time-dependent curve was performed by using bovine serum albumin (BSA) to

https://doi.org/10.1021/acsomega.4c06577
ACS Omega 2025, 10, 10826−10834

simulate the controlled release of rhBMP2 by the BMP@ZIF hydrogel. Before gelation, 100 mg of BSA was incorporated into the hydrogel precursor solution. Initially, the samples were immersed in 1 mL of PBS solution containing 0.1% (v/w) sodium azide (NaN_3) (Sigma−Aldrich). BSA released from hydrogels was assessed in 50 μL of the PBS collected from each sample's supernatant at days 0, 1, 3, 7, 14, and 28. A protein quantification kit calculated the amount of BSA released at each time interval according to the manufacturer's instructions (Thermo Fisher Scientific). The following equation was used to obtain the BSA percentage release

$$\text{Releasing percentage (\%) at day t} = \frac{\text{BSA content on day t}}{\text{Initial BSA content}} \times 100\%$$

2.6. Cell Culture. Human Dental Pulp stemcells (DPSCs) were isolated as previously described. Cells were expanded in α-MEM supplemented with 15% of Fetal Bovine Serum (FBS), 4 mM of L-Glutamine, and 50 IU/mL of penicillin/streptomycin at 37 °C in a humid atmosphere containing 5% CO_2. DPCs from the fourth passage were used for hydrogel encapsulation at a density of 5×10^6/mL. All hydrogels were cultured with osteogenic media containing 10 mM β-glycerophosphate disodium, 50 mg/mL L-ascorbic acid 2-phosphate magnesium salt hydrate, and 100 nM dexamethasone for 7 days. Osteogenic media were changed every other day. To assess the osteogenic differentiation, samples were analyzed by the relative expression and immunofluorescence staining of osteogenic markers.

2.7. Immunofluorescence Staining. At day 3, immunofluorescence staining was performed to assess the expression of encapsulated cells for cell adhesion and osteogenic markers. First, the hydrogels were fixed in 4% (w/v) paraformaldehyde solution (PFA) for 15 min. The samples were rinsed with PBS solution, permeabilized with 0.25% Triton-X100 PBS, and incubated in a blocking buffer containing 1% BSA PBS for 45 min. The hydrogels were incubated overnight, at 4 °C, in a blocking buffer containing the following primary antibodies: integrin-β1 (1:100) and osteocalcin (1:100) (Abcam). The next day, samples were rinsed with 0.5% Tween 20 in PBS and incubated in blocking buffer containing secondary antibodies (1:400, Thermo Fisher). After washing with 0.5% Tween 20 PBS, the nuclei were counterstained with DAPI (1:1000; Molecular Probes, Eugene, OR, USA). Image acquisition was performed using a Leica SP8 confocal microscope (Wetzlar, German). The same exposure conditions were applied to all of the experimental groups.

2.8. Real-Time Quantitative Polymerase Chain Reaction. We used real-time quantitative polymerase chain reaction (RTq-PCR) to analyze the gene expression of encapsulated DPCs on the seventh day. Total RNA was with the TRIzol reagent (Invitrogen, Carlsbad, CA, USA) following the manufacturer's instructions. For each sample, 100 ng of mRNA was transcribed into cDNA using the RevertAid First Strand cDNA synthesis kit following the manufacturer's instructions (Thermo Fisher). For each condition, quantitative gene expression was obtained by combining SYBR Green master mix (Thermo Fisher) and the following primers (Table 1) for osteogenic genes: mitogen-activated protein kinase (MAPK), alkaline phosphatase (ALP), collagen type I (Col1), osteocalcin (OCN), runt-related transcription factor 2 (RUNX 2), and glyceraldehyde-3-phosphate dehydrogenase (GAPDH) (all from Thermo Fisher Scientific). The $2^{-\Delta\Delta CT}$ method was used to assess the relative gene expression fold change. The GelMA group was used as the reference control (1-fold).

Table 1. Human Primer Sequences Used for RT-qPCR Analysis

gene	primers
MAPK	forward: TACACCAACCTCTCGTACATCG reverse: CATGTCTGAAGCGCAGTAAGATT
ALP	forward: ACCACCACGAGAGTGAACCA reverse: CGTTGTCTGAGTACCAGTCCC
Col 1	forward: GAGGGCCAAGACGAAGACATC reverse: CAGATCACGTCATCGCACAAC
OCN	forward: CACTCCTCGCCCTATTGGC reverse: CCCTCCTGCTTGGACACAAAG
RUNX2	forward: TGGTTACTGTCATGGCGGGTA reverse: TCTCAGATCGTTGAACCTTGCTA
GAPDH	forward: GGAGCGAGATCCCTCCAAAAT reverse: GGCTGTTGTCATACTTCTCATGG

2.9. Statistical Analysis. The comparison of fits of each curve of storage modulus was compared by nonlinear regression (Extra sum-of-squares F Test). The Shapiro−Wilk test was performed to evaluate the data distribution. RT-qPCR was analyzed by ANOVA, followed by Tukey's multiple comparison tests for comparison among groups. All data was analyzed at a level of significance of 5%. The software used for this analysis was GraphPad Prism 9 (GraphPad Software Inc., La Jolla, CA, USA).

3. RESULTS

3.1. BMP@ZIF@GelMA Showed Sustained Release of BMP. We loaded 1 μg of BMP-2 into ZIF-8 nanoparticles, which were subsequently encapsulated within the hydrogels. The morphology and size of the BMP-2-loaded nanoparticles, ranging from 40 to 60 nm, were characterized using TEM (Figure S1), while their crystalline structure was confirmed through XRD analysis (Figure S2). Upon examination of the structural morphology of hydrogels, it became evident that both ZIF@GelMA and BMP@ZIF@GelMA exhibited a porous structure that closely resembled that of GelMA (Figure 1A,B). This porous nature was indicative of spaces or voids within the material, allowing for a range of biological applications and functionalities. Furthermore, the distribution of BSA-FITC@ZIF nanoparticles within the GelMA hydrogels (Figure S3) demonstrates a uniform dispersion of protein-loaded nanoparticles throughout the hydrogel matrix. This even distribution is critical for ensuring consistent delivery and release of the encapsulated proteins, thereby enhancing the hydrogel's functionality for potential therapeutic applications.

The behavior of the modified hydrogels tended to align closely with that of the control sample, suggesting consistent viscoelastic characteristics across the samples (Figure 1C). Notably, the BMP@ZIF@GelMA sample stood out, as its G' value, which represented the elastic modulus, was higher when the curves were compared ($p < 0.001$). This indicated that the BMP@ZIF@GelMA hydrogel had an enhanced ability to store energy elastically in higher frequency zones (10 to 100 rads/s), making it more deformation resistant than the other samples. At low frequency, all samples performed similarly and corresponded to the expect molecular conformation of general hydrogels.

BSA was used as a model protein to study the degradation and release pattern of the BSA@ZIF@GelMA hydrogel over 28 days (Figure 1D,E). The BSA@ZIF@GelMA hydrogel

https://doi.org/10.1021/acsomega.4c06577
ACS Omega 2025, 10, 10826−10834

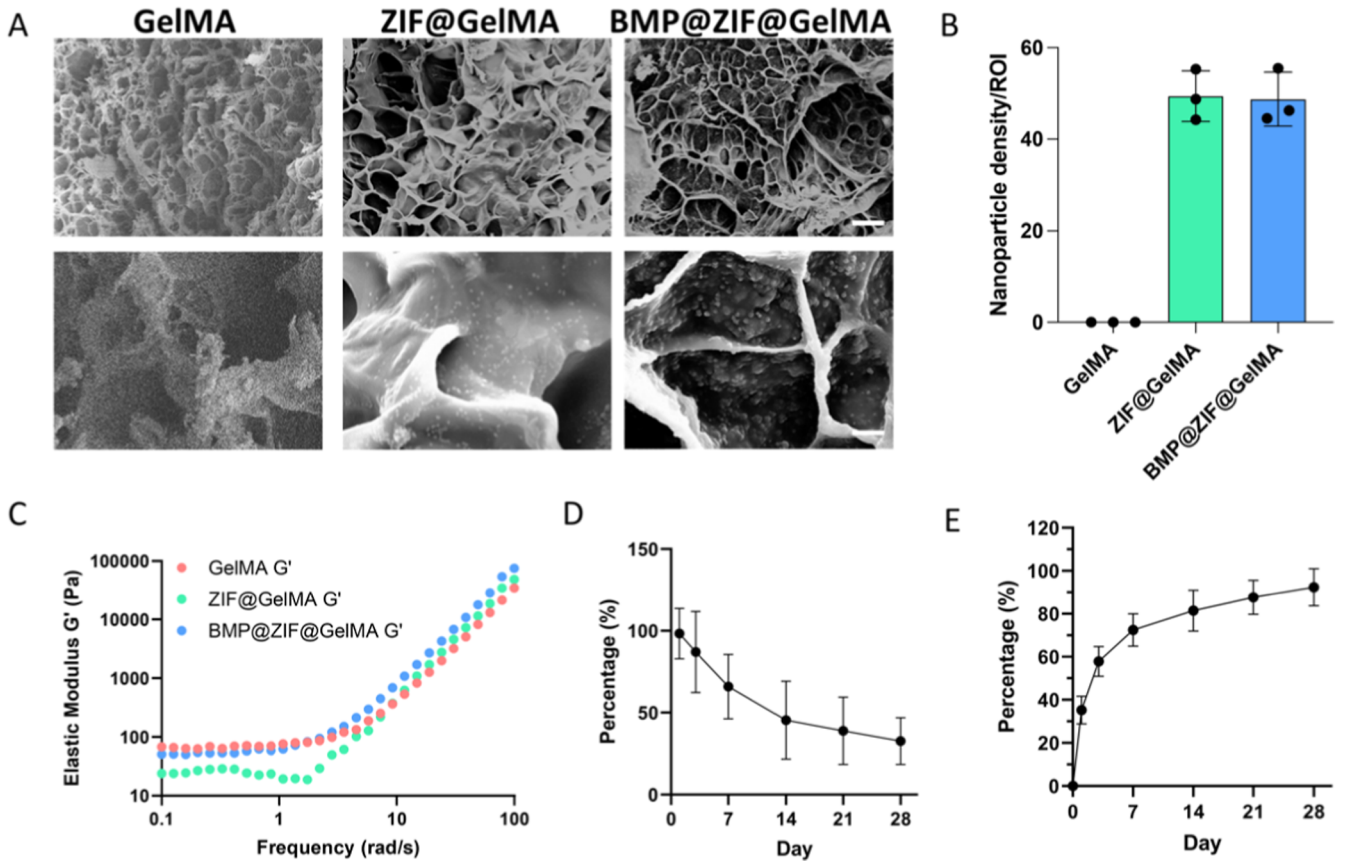

Figure 1. (A) SEM images of GelMA, ZIF@GelMA, and BMP@ZIF@GelMA obtained at 1000 (upper images) and 5000 (lower images) magnifications. Scale bar: 100 μm (top); 20 μm (bottom). (B) Quantification of nanoparticle density in ROI. (C) Rheological test of GelMA, ZIF@GelMA, and BMP@ZIF@GelMA. (D) Degradation and (E) release percentage of BSA from BMP@ZIF@GelMA samples over 28 days.

demonstrated a balanced degradation rate. Accordingly, by the 14th day, approximately half of the hydrogel had degraded, indicating a degradation percentage of around 50%. Following this, the degradation pace moderated, ensuring the hydrogel's continued presence to support eventual bone regeneration. We also evaluated the release pattern of BSA from the BSA@ZIF@GelMA hydrogel over the same period (Figure 3B). The data suggest a sustained and controlled release of BSA, with a gradual and progressive release as time progressed.

3.2. Encapsulated hMSCs in BMP@ZIF@GelMA Show More Significant Expression of Integrin β-1 and Osteocalcin. We provided a comprehensive visualization of Figure 2 depicting the expression levels of two reparative markers, Integrin β-1 and Osteocalcin, in cells encapsulated within the hydrogels. When examining the ZIF@GelMA hydrogel, there's a noticeable upregulation in the expression of both Integrin b-1 and Osteocalcin compared to the control group, which utilized the GelMA hydrogel. This heightened expression suggests that the ZIF@GelMA hydrogel might offer a more conducive environment for cellular activities related to bone formation and cell adhesion, as indicated by the elevated levels of these markers. Furthermore, when BMP-2 was introduced into the ZIF@GelMA hydrogel, the expression levels of the markers were further upregulated. This indicates that the addition of BMP-2 significantly promoted the expression of Integrin β-1 and Osteocalcin.

3.3. BMP@ZIF@GelMA Showed Greater Biomineral Deposition and Expression of Osteogenic Markers. We further provided an in-depth representation of the relative gene expression associated with osteogenic markers and cell adhesion. Both ALP activity assay and alizarin red staining showed that the BMP@ZIF@GelMA group showed the highest expression level and deposition of biominerals (Figure 3A,B). Within the BMP@ZIF@GelMA hydrogel samples, DPCs exhibited a pronounced expression of several pivotal markers for osteogenesis, such as MAPK, ALP, Col1, OCN, and RUNX 2, when compared to GelMA ($p < 0.001$ or lower) and ZIF NP ($p < 0.01$ or lower) groups (Figure 3C). These genes play crucial roles in various cellular processes, including bone mineralization, matrix formation, and cellular differentiation, underscoring the potential efficacy of BMP@ZIF@GelMA hydrogels in promoting osteogenesis. Conversely, hydrogels that incorporated only ZIF NPs without adding BMP exhibited gene expression levels mostly similar to those observed in the control group ($p > 0.05$). ALP, Col 1, and OCN mRNA were unregulated for ZIF NPs compared to GelMA (control) ($p < 0.01$ or lower). This suggests that while ZIF incorporation provides a scaffold and structure to the hydrogel, it might not inherently enhance or stimulate the expression of osteogenic and adhesion-related genes to the same extent as when BMP is also present.

4. DISCUSSION

Tissue engineering shifts the research directions to create therapeutical approaches able to substitute or regenerate functional bone-lost tissue, particularly in craniofacial injuries.[54−56] We demonstrated that the ZIF-modified hydrogels without or in association with BMP-2 can upregulate bone

https://doi.org/10.1021/acsomega.4c06577
ACS Omega 2025, 10, 10826−10834

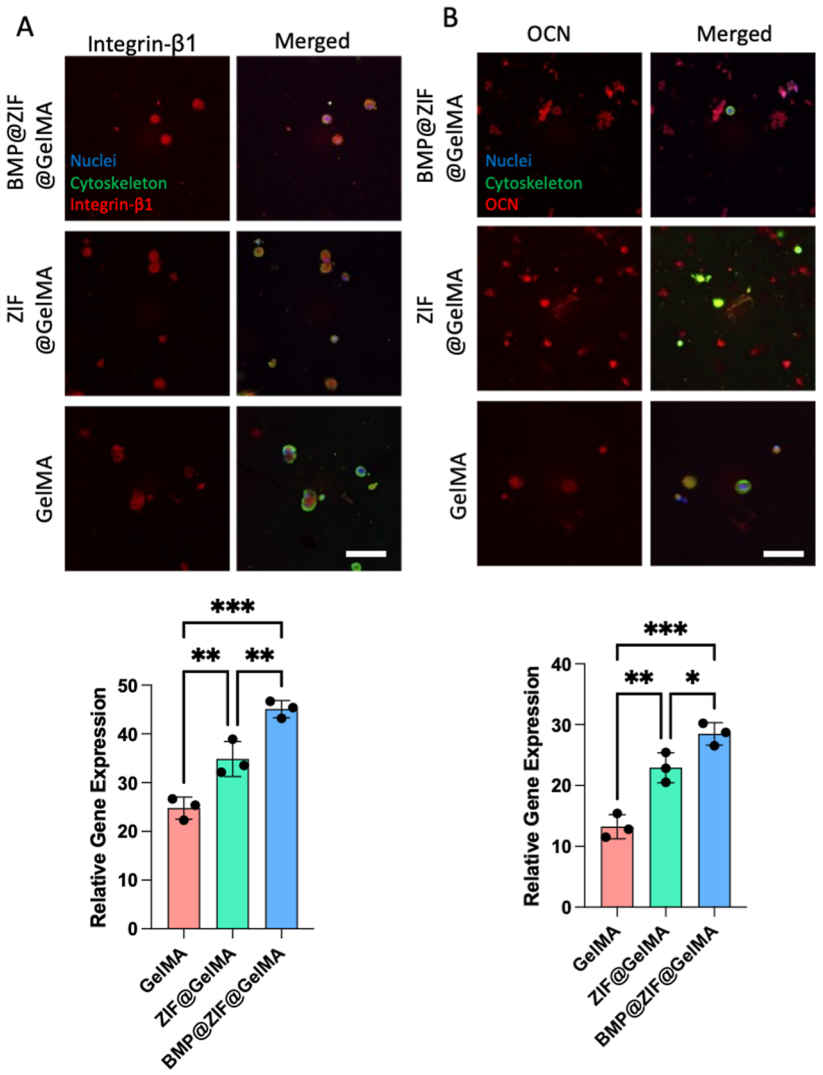

Figure 2. Immunofluorescence staining of encapsulated hMSCs of (A) Integrin β-1 and (B) OCN. Blue: Nuclei. Green: cytoskeleton. Red: Integrin-β1/OCN. Scale bar: 10 μm.

formation genes and release molecules sustainably while being slowly degraded. Previous reports showed that the Zn^{2+} ion is involved in activating MAPK and AKT pathways, in addition to promote angiogenesis, osteogenesis, and antibacterial properties.[57,58]

Hydrogel viscoelastic properties are crucial for mimicking the extracellular matrix (ECM). We observed a significant storage modulus increase for the BMP@ZIF@GelMA nanocomposite hydrogels, suggesting potential advantages in resilience and structural integrity demands. Porous structures are one of the requirements for bone tissue engineering scaffolds, making them ideal carriers. Furthermore, slow and controlled degradation of hydrogels is critical due to the required time for physiological and repairing processes. A moderate degradation rate ensures that the hydrogel remains in the targeted area for an optimal duration, providing a scaffold for the growth and maturation of new bone cells to grow and mature. A balanced degradation rate is primordial, because if the hydrogel degrades too quickly, it may not provide adequate support for bone growth. At the same time, if it degrades too slowly, it might hinder the natural bone remodeling process. Gelatin hydrogels are biodegradable and present a sustained release of drugs. Our results demonstrated that our modified hydrogel property, therefore, is advantageous as it ensures consistent availability of therapeutic agents or proteins, like rhBMP-2, which may guide the bone regeneration process and enhance the success rate of the treatment.

In dealing with bone tissue engineering, hydrogels must have the following properties: biocompatibility and osteoinductive and osteoconductive properties. Previous work reported modifying a catechol-chitosan hydrogel incorporating ZIF-8 to promote osteogenesis and accelerate bone repair.[59] According to our findings, the release of BMP-2 from ZIF-8 nanoparticles upregulated the production of osteogenic markers, such as alkaline phosphatase, collagen 1, and osteocalcin. More recently, a bioactive glass loaded with ZIF-8 and BMP-2 association showed a sustained release of the bioactive molecules and, at the same time, enhanced osteoblast in vitro adhesion and proliferation and osteogenic differentiation toward bone repair in vivo.[60,61] Besides bone repair, it was already demonstrated in vitro the ability of these nanoparticles to activate an acute inflammatory response and macrophage polarization toward the M2 type, suggesting an application for wound repair.

https://doi.org/10.1021/acsomega.4c06577
ACS Omega 2025, 10, 10826−10834

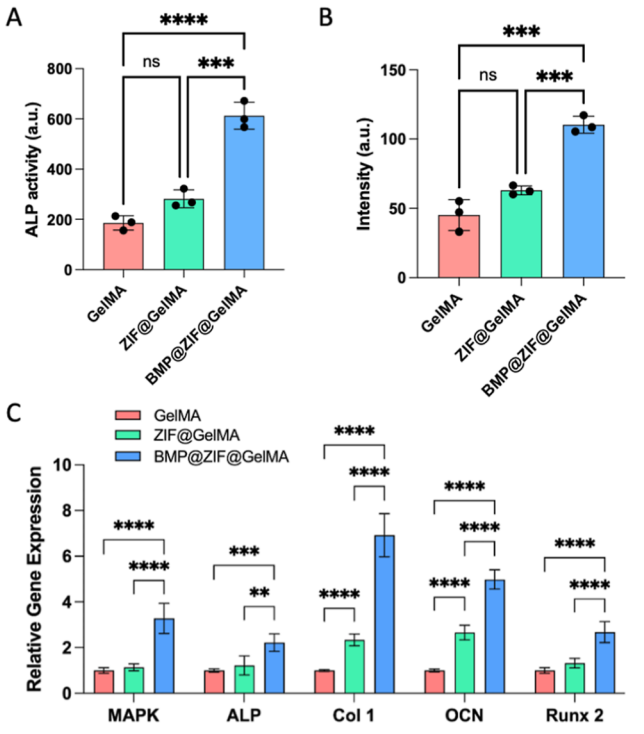

Figure 3. (A) ALP activity assay. (B) Intensity of biominerals stained by alizarin red. (C) Bar graphs showing RT-qPCR analysis for selected osteogenic markers. All groups were compared by ANOVA followed by Tukey's posthoc test (*$p < 0.05$; **$p < 0.01$; $p < 0.001$; ****$p < 0.0001$). GelMA = 1-fold change.

Previous reports demonstrated that ZIF-8 addition improved the interface between a catechol-functionalized chitosan (CA-CS) polymer matrix, increasing its mechanical properties.[59] Within the ZIF groups, there was a noticeable presence of nanoparticles embedded in the hydrogel matrix. These nanoparticles were not merely dispersed but were intricately incorporated into the hydrogel network. This suggested a deliberate design choice to enhance the hydrogel properties or functionalities. Such nanoparticle incorporation could have influenced the mechanical strength, responsiveness, or possibly other vital physicochemical properties of hydrogels, warranting further investigation.

While we conducted preliminary short-term in vitro analyses focused on the physical properties of hydrogels and osteoinductive potential, the study has some limitations, particularly the lack of long-term data on protein interactions and cell differentiation. Future studies will need to address these limitations by conducting in vivo experiments, where the long-term therapeutic potential and biodegradability of the hydrogels can be fully assessed. Additionally, more detailed physicochemical characterization of the rhBMP-2 functionalization and its sustained release profile could optimize the biomaterial's therapeutic efficacy. Looking ahead, BMP@ZIF@GelMA hydrogels offer exciting prospects for advanced therapeutic applications, particularly in promoting angiogenesis and modulating the immune response in inflammatory environments. Future research will explore the use of this hydrogel in animal models with critical bone defects as well as the delivery of other bioactive molecules to further enhance the overall regenerative outcome. These studies will provide a deeper understanding of the long-term effects of hydrogels and pave the way for clinical applications in bone tissue engineering and regenerative medicine.

5. CONCLUSIONS

The integration of ZIF NPs into GelMA hydrogels demonstrated significant potential for bone tissue engineering by supporting the controlled protein release and promoting osteogenic differentiation. The BMP@ZIF@GelMA hydrogel, in particular, exhibited a balanced degradation rate and sustained release of rhBMP-2, which were critical for driving cellular adhesion and osteogenic differentiation. Short-term analyses revealed that dental pulp cells encapsulated within the BMP@ZIF@GelMA hydrogel showed a marked upregulation of key osteogenic markers, underscoring its ability to create a favorable microenvironment for bone regeneration. These findings highlight the potential of the BMP@ZIF@GelMA hydrogel to support sustained tissue repair and regeneration by delivering therapeutic molecules effectively while maintaining structural integrity. Future studies are needed to evaluate the long-term in vivo performance and explore the incorporation of additional bioactive molecules to further enhance the therapeutic versatility. The BMP@ZIF@GelMA hydrogel offers an innovative approach to addressing complex bone defects, making it a promising candidate for advanced applications in regenerative medicine and tissue engineering.

■ ASSOCIATED CONTENT

Data Availability Statement

The data supporting the findings of this study are fully disclosed in this manuscript.

Supporting Information

The Supporting Information is available free of charge at https://pubs.acs.org/doi/10.1021/acsomega.4c06577.

Details of ZIF-8 nanoparticle design, TEM results of nanoparticle morphology, XRD analysis confirming crystalline structure, distribution analysis of BSA-FITC@ZIF nanoparticles in GelMA hydrogels, and comparative analysis of ZIF-8-based nanocomposites in bone tissue engineering (PDF)

■ AUTHOR INFORMATION

Corresponding Author

Alireza Moshaverinia − *Weintraub Center for Reconstructive Biotechnology, Section of Prosthodontics, School of Dentistry, University of California, Los Angeles, California 90095, United States;* orcid.org/0000-0002-1542-6202; Phone: (310) 794-6324; Email: amoshaverinia@ucla.edu

Authors

Weihao Yuan − *Weintraub Center for Reconstructive Biotechnology, Section of Prosthodontics, School of Dentistry, University of California, Los Angeles, California 90095, United States*

Luiza de Almeida Queiroz Ferreira − *Weintraub Center for Reconstructive Biotechnology, Section of Prosthodontics, School of Dentistry, University of California, Los Angeles, California 90095, United States; Department of Restorative Dentistry, School of Dentistry, Universidade Federal de Minas Gerais, Belo Horizonte, Minas Gerais 31270-901, Brazil*

Ronit Khade − *Weintraub Center for Reconstructive Biotechnology, Section of Prosthodontics, School of Dentistry,*

https://doi.org/10.1021/acsomega.4c06577
ACS Omega 2025, 10, 10826−10834

University of California, Los Angeles, California 90095, United States

Ivana Diniz − *Weintraub Center for Reconstructive Biotechnology, Section of Prosthodontics, School of Dentistry, University of California, Los Angeles, California 90095, United States; Department of Restorative Dentistry, School of Dentistry, Universidade Federal de Minas Gerais, Belo Horizonte, Minas Gerais 31270-901, Brazil*

Sahar Ansari − *Weintraub Center for Reconstructive Biotechnology, Section of Prosthodontics, School of Dentistry, University of California, Los Angeles, California 90095, United States*

Complete contact information is available at: https://pubs.acs.org/10.1021/acsomega.4c06577

Author Contributions

[§]Weihao Yuan and Luiza de Almeida Querioz Ferraira contributed equally to the study.

Notes

The authors declare no competing financial interest.

■ ACKNOWLEDGMENTS

This study was financed in part by the Coordenação de Aperfeiçoamento de Pessoal de Nível Superior (CAPES)−Finance Code 001 (Scholarship for Dr. Ferreira and Dr. Diniz).

■ REFERENCES

(1) Kamalakar, A.; Tobin, B.; Kaimari, S.; Robinson, M. H.; Toma, A.; Cha, T.; Chihab, S.; Moriarity, I.; Gautam, S.; Bhattaram, P.; et al. Delivery of a Jagged1-PEG-MAL hydrogel with pediatric human bone cells regenerates critically sized craniofacial bone defects. *Elife* **2024**, *13*, RP92925.

(2) Kim, M.; Wang, X. L.; Li, Y. M.; Lin, Z. T.; Collins, C. P.; Liu, Y. G.; Ahn, Y.; Tsal, H. M.; Song, J. W.; Duan, C. W.; et al. Personalized composite scaffolds for accelerated cell- and growth factor-free craniofacial bone regeneration. *Bioact. Mater.* **2024**, *41*, 427−439.

(3) Liao, S. N.; Li, S. H.; Liu, Z. Q.; Lu, W. T.; He, Y. T.; Xia, K.; Wang, Y. G.; Zhao, Z. H.; Lin, Y. F. A bioswitchable siRNA delivery system: RNAi therapy based on tetrahedral framework nucleic acids for bone defect repair. *Nanoscale* **2024**, *16*, 21531.

(4) Romanowicz, G. E.; Zhang, L. Z.; Bolger, M. W.; Lynch, M.; Kohn, D. H. Beyond bone volume: Understanding tissue-level quality in healing of maxillary vs. femoral defects. *Acta Biomater.* **2024**, *187*, 409−421.

(5) Zheng, Y.; Tan, L.; Chen, H.; He, S. H.; Li, M. H.; Luo, Z.; Cai, K. Y.; Hu, Y. Hierarchical Integration of Curcumin-Loaded $CaCO_3$ Nanoparticles and Black Phosphorus Nanosheets in Core/Shell Nanofiber for Cranial Defect Repair. *Adv. Healthcare Mater.* **2024**, *13*, 2401786.

(6) Griffin, M.; Kalaskar, D. M.; Butler, P. E.; Seifalian, A. M. The Use of Adipose Stem Cells in Cranial Facial Surgery. *Stem Cell Rev. Rep.* **2014**, *10* (5), 671−685.

(7) Pourlak, T.; Pourlak, T.; Ghodrati, M.; Mortazavi, A.; Dolati, S.; Yousefi, M. Usage of stem cells in oral and maxillofacial region. *J. Stomatol. Oral Maxillofac. Surg.* **2021**, *122* (4), 441−452.

(8) Kirmanidou, Y.; Chatzinikolaidou, M.; Michalakis, K.; Tsouknidas, A. Clinical translation of polycaprolactone-based tissue engineering scaffolds, fabricated via additive manufacturing: A review of their craniofacial applications. *Biomater. Adv.* **2024**, *162*, 213902.

(9) Liu, Y. J.; Li, L.; He, M. J.; Xu, Y. M.; Wu, Z. K.; Xu, X. C.; Luo, K.; Lv, H. B. Self-assembled peptide hydrogel loaded with functional peptide Dentonin accelerates vascularized bone tissue regeneration in critical-size bone defects. *Regener. Biomater.* **2024**, *11*, rbae106.

(10) Evrard, R.; Manon, J.; Maistriaux, L.; Fievé, L.; Darius, T.; Cornu, O.; Lengelé, B.; Schubert, T. Enhancing the biological integration of massive bone allografts: A porcine preclinical in vivo pilot-study. *Bone* **2024**, *187*, 117213.

(11) Li, W. R.; Luo, Y.; Zhao, X. B.; Wang, J. L. Meniscal Allograft versus Synthetic Graft in Treatment Outcomes of Meniscus Repair: A Mini-review and Meta-analysis. *ACS Biomater. Sci. Eng.* **2024**, *10* (8), 4757−4770.

(12) Semitela, A.; Marques, P. A. A. P.; Completo, A. Strategies to engineer articular cartilage with biomimetic zonal features: a review. *Biomater. Sci.* **2024**, *12* (23), 5961−6005.

(13) Chen, Z. G.; Wang, X.; Liu, J.; Liu, K. Z.; Li, S.; Wu, M. M.; Wu, Z. Q.; Wang, Z. M.; Shi, Y.; Ruan, C. S. A Stone-Cottage-Inspired Printing Strategy to Build Microsphere Patterned Scaffolds for Accelerated Bone Regeneration. *Adv. Funct. Mater.* **2024**, 2417836.

(14) Tan, S. L.; Luo, X. H.; Wang, Y. F.; Chen, S. S.; Jiang, T.; Yang, X. S.; Peng, X. Y.; Zhang, X. Y.; Zhang, S.; Zhang, C. F.; et al. Biomimetic non-collagenous proteins-calcium phosphate complex with superior osteogenesis regulating macrophage IL-27 secretion. *Biomaterials* **2025**, *315*, 122917.

(15) Whitman, M. A.; Mantri, M.; Spanos, E.; Estroff, L. A.; De Vlaminck, I.; Fischbach, C. Bone mineral density affects tumor growth by shaping microenvironmental heterogeneity. *Biomaterials* **2025**, *315*, 122916.

(16) Yin, M. T.; Liu, Z. Q.; Sun, Z. Y.; Qu, X. Y.; Chen, Z. Y.; Diao, Y. Y.; Cheng, Y. X.; Shen, S. S.; Wang, X. S.; Cai, Z. Y.; et al. Biomimetic Scaffolds Regulating the Iron Homeostasis for Remolding Infected Osteogenic Microenvironment. *Adv. Sci.* **2024**, *11*, 2407251.

(17) Zhang, Y. J.; Liu, Y.; Li, Z. C.; Zhang, Q.; Li, J. C. Breast Cancer Bone Metastasis Therapy and Tumor-Associated Bone Destruction Repair by Versatile Semiconducting Nanointegrators with X-Ray Adjuvant. *Adv. Funct. Mater.* **2025**, *35*, 2412165.

(18) Huang, Y. Q.; Du, Z. Y.; Wei, P. F.; Chen, F. Y.; Guan, B. B.; Zhao, Z. D.; Zhang, X.; Cai, Q.; Mao, J. P.; Leng, H. J.; et al. Biodegradable microspheres made of conductive polyorganophosphazene showing antioxidant capacity for improved bone regeneration. *Chem. Eng. J.* **2020**, *397*, 125352.

(19) Yadav, N.; Kumar, U.; Roopmani, P.; Krishnan, U. M.; Sethuraman, S.; Chauhan, M. K.; Chauhan, V. S. Ultrashort Peptide-Based Hydrogel for the Healing of Critical Bone Defects in Rabbits. *ACS Appl. Mater. Interfaces* **2022**, *14* (48), 54111−54126.

(20) Zhu, X. J.; Wang, C. Y.; Bai, H. T.; Zhang, J. X.; Wang, Z. H.; Li, Z. H.; Zhao, X.; Wang, J. C.; Liu, H. Functionalization of biomimetic mineralized collagen for bone tissue engineering. *Mater. Today Bio* **2023**, *20*, 100660.

(21) Abdal-hay, A.; Xiang, E. M.; Khodary, F.; Ivanovski, S. Fabrication of ZnO-loaded, polycaprolactone -based, antibacterial 3D scaffolds for bone tissue engineering using melt-electrowriting. *Mater. Lett.* **2025**, *379*, 137580.

(22) Peng, B.; Mohammed, F. S.; Tang, X. J.; Liu, J.; Sheth, K. N.; Zhou, J. B. Nanotechnology approaches to drug delivery for the treatment of ischemic stroke. *Bioact. Mater.* **2025**, *43*, 145−161.

(23) Wang, Y. J.; Liu, C. R.; Fang, C.; Peng, Q. X.; Qin, W.; Yan, X. B.; Zhang, K. Engineered Cancer Nanovaccines: A New Frontier in Cancer Therapy. *Nano-micro Lett.* **2025**, *17* (1), 30.

(24) Li, G. L.; Gao, F.; Yang, D. L.; Lin, L.; Yu, W. J.; Tang, J. Q.; Yang, R. H.; Jin, M.; Gu, Y. T.; Wang, P. F.; et al. ECM-mimicking composite hydrogel for accelerated vascularized bone regeneration. *Bioact. Mater.* **2024**, *42*, 241−256.

(25) Wang, S. J.; Deng, R. H.; Song, C. H.; Yuan, F. Z.; Li, P. Q.; Cao, X. Y.; Wang, X.; Lin, L.; Zhang, J. Y.; Zhu, Y. F.; et al. Biomechanically matched and multistage hybrid porous scaffolds for stem cell-based osteochondral regeneration. *Nano Today* **2024**, *59*, 102539.

(26) Zhan, Z. H.; Li, R.; Wu, Y.; Shen, X. T.; Fu, D. M.; Han, H.; Jing, P. R.; Li, B.; Han, F. X.; Meng, B. Biomimetic periosteum-bone scaffolds with codelivery of BMP-2 and PDGF-BB for skull repair. *Bone* **2025**, *190*, 117315.

(27) Chen, S. Q.; Xie, Y.; Ma, K.; Wei, Z. W.; Ran, X. W.; Fu, X. B.; Zhang, C. P.; Zhao, C. S. Electrospun nanofibrous membranes meet antibacterial nanomaterials: From preparation strategies to biomedical applications. *Bioact. Mater.* **2024**, *42*, 478−518.
(28) Chen, X.; Wu, Y. L.; Song, P.; Feng, L. D.; Zhou, Y.; Shi, J. W.; Dong, N. G.; Qiao, W. H. Matrix Metalloproteinase-Responsive Controlled Release of Self-Assembly Nanoparticles Accelerates Heart Valve Regeneration In Situ by Orchestrating Immunomodulation. *Adv. Sci.* **2025**, *12*, 2403351.
(29) Yang, D. J.; Liu, K.; Cai, C. Y.; Xi, J. J.; Yan, C. M.; Peng, Z. L.; Wang, Y. L.; Jing, L.; Zhang, Y.; Xie, F.; et al. Target-Engineered Liposomes Decorated with Nanozymes Alleviate Liver Fibrosis by Remodeling the Liver Microenvironment. *ACS Appl. Mater. Interfaces* **2024**, *16*, 64536.
(30) Yun, J.; Woo, H. T.; Lee, S.; Cha, H. J. Visible light-induced simultaneous bioactive amorphous calcium phosphate mineralization and crosslinking of coacervate-based injectable underwater adhesive hydrogels for enhanced bone regeneration. *Biomaterials* **2025**, *315*, 122948.
(31) Zhang, Z. B.; Li, C. F.; Guo, J.; Liu, T. J.; Zhang, W. Y.; Bai, S. Z.; Li, B.; Zhao, Y. M.; Xu, F.; Wang, W. "Young-Mechanical Niche" biomimetic hydrogel promotes dental pulp regeneration through YAP-dependent mechanotransduction. *Chem. Eng. J.* **2024**, *501*, 157483.
(32) Zhao, F. L.; Jia, Z. B.; Zhang, L. Y.; Liu, G. D.; Li, J. F.; Zhao, J. M.; Xie, Y. J.; Chen, L.; Jiang, H. Y.; He, W.; et al. A MnO2 nanosheets doping double crosslinked hydrogel for cartilage defect repair through alleviating inflammation and guiding chondrogenic differentiation. *Biomaterials* **2025**, *314*, 122875.
(33) Pan, G. Y.; Li, M.; Mu, L.; Huang, Y.; Liang, Y. P.; Guo, B. L. Photothermal/Photodynamic Synergistic Antibacterial Hydrogel Dressing with pH/Glucose Dual Responsive Pirfenidone Release for Diabetic Foot Ulcers. *Adv. Funct. Mater.* **2024**, 2416205.
(34) Wang, Y.; Chen, C.; He, C. Y.; Dong, W. T.; Yang, X. K.; Kong, Q. Q.; Yan, B.; He, J. Quaternized chitosan-based biomimetic nanozyme hydrogels with ROS scavenging, oxygen generating, and antibacterial capabilities for diabetic wound repair. *Carbohydr. Polym.* **2025**, *348*, 122865.
(35) Xie, Y. X.; Li, G. C.; Wu, J.; Zhu, J. C.; Cai, X. M.; Zhao, P. Z.; Zhang, D.; Zhong, Y. Injectable self-healing alginate/PEG hydrogels cross-linked via thiol-Michael addition bonds for hemostasis and wound healing. *Carbohydr. Polym.* **2025**, *348*, 122864.
(36) Deng, D. K.; Li, X.; Zhang, J. J.; Yin, Y.; Tian, Y.; Gan, D.; Wu, R. X.; Wang, J.; Tian, B. M.; Chen, F. M.; et al. Biotin-Avidin System-Based Delivery Enhances the Therapeutic Performance of MSC-Derived Exosomes. *ACS Nano* **2023**, *17* (9), 8530−8550.
(37) Qi, L.; Hong, S. B.; Zhao, T.; Yan, J.; Ge, W. W.; Wang, J.; Fang, X.; Jiang, W. D.; Shen, S. G. F.; Zhang, L. DNA Tetrahedron Delivering miR-21−5p Promotes Senescent Bone Defects Repair through Synergistic Regulation of Osteogenesis and Angiogenesis. *Adv. Healthcare Mater.* **2024**, *13*, 2401275.
(38) Wang, J. L.; Huang, D. Q.; Ren, H. Z.; Shang, L. R. Biomimic Trained Immunity-MSCs Delivery Microcarriers for Acute Liver Failure Regeneration. *Small* **2022**, *18* (36), 2200858.
(39) Xu, P. P.; Lou, L. B.; Zhan, W. D.; Wang, C. Y.; Wu, S. S.; Liu, Z. W.; Wang, Y. X. Bicomponent hydrogel laden with TGF-I33-nucleus pulposus stem cells for disc degeneration repair. *Chem. Eng. J.* **2024**, *479*, 147788.
(40) Zheng, B. W.; Yang, L. A.; Feng, S. N.; Zhu, Y. M.; Du, L. J.; Zhang, J. R.; Huang, J. F.; Le, D. M. J.; Miao, Y.; Hu, Z. Q. Organoid-Loaded Cryomicroneedles for Biomimic Hair Regeneration. *Adv. Funct. Mater.* **2024**, *34* (3), 2304950.
(41) Abdelhamid, H. N. Zeolitic Imidazolate Frameworks (ZIF-8) for Biomedical Applications: A Review. *Curr. Med. Chem.* **2021**, *28* (34), 7023−7075.
(42) Wang, Z.; Qi, L.; Huang, Y.; Liu, Z.; Wu, R. B.; Zhao, Y. Z.; Li, H.; Wang, S. Y.; Liu, L. M.; Zhang, L.; et al. Stem Cell Membrane-Camouflaged Biomimetic Nanoparticles Inhibiting Leptin Pathway for Intervertebral Disc Degeneration Therapy. *ACS Appl. Mater. Interfaces* **2024**, *16* (46), 63333−63344.
(43) Xiang, J.; Zhou, X. M.; Xia, Z. M.; Zhang, Z. M.; Xu, K.; Hu, S. S.; Zhang, Z. Z.; Liu, J. Q.; Yang, W.; Yu, L. X.; et al. All-trans retinoic acid-functionalized injectable hydrogel with immunomodulation, osteogenesis and antibacterial capability for periodontitis therapy. *Chem. Eng. J.* **2024**, *500*, 156915.
(44) Yang, Y.; Wang, W. M.; Zeng, Q. R.; Wang, N.; Li, W. B.; Chen, B.; Guan, Q. X.; Li, C. Y.; Li, W. Fabricating oxygen self-supplying 3D printed bioactive hydrogel scaffold for augmented vascularized bone regeneration. *Bioact. Mater.* **2024**, *40*, 227−243.
(45) Hoseinpour, V.; Shariatinia, Z. Applications of zeolitic imidazolate framework-8 (ZIF-8) in bone tissue engineering: A review. *Tissue Cell* **2021**, *72*, 101588.
(46) Nezhad-Mokhtari, P.; Rahbarghazi, R.; Hamishehkar, H.; Asadi, P.; Milani, M. Innovative Nanocomposite Scaffolds Containing ZIF-8 Nanoparticles for Improving Wound Healing: A Review. *J. Polym. Environ.* **2024**, *32*, 6211.
(47) Zhang, X.; Chen, J. Y.; Pei, X.; Yang, L. X.; Wang, L.; Chen, L. N.; Yang, G. M.; Pei, X. B.; Wan, Q. B.; Wang, J. Drug-loading ZIF-8 for modification of microporous bone scaffold to promote vascularized bone regeneration. *Chin. Chem. Lett.* **2024**, *35* (6), 108889.
(48) Fernandez-Yague, M. A.; Palma, M.; Tofail, S. A. M.; Duffy, M.; Quinlan, L. R.; Dalby, M. J.; Pandit, A.; Biggs, M. J. A Tympanic Piezo-Bioreactor Modulates Ion Channel-Associated Mechanosignaling to Stabilize Phenotype and Promote Tenogenesis in Human Tendon-Derived Cells. *Adv. Sci.* **2024**, *11*, 2405711.
(49) He, S. K.; Hu, R. N.; Yao, X.; Cui, J.; Liu, H. M.; Zhu, M.; Ning, L. J. The effects of heat and hydrogen peroxide treatment on the osteoinductivity of demineralized cortical bone: a potential method for preparing tendon/ligament repair scaffolds. *Regener. Biomater.* **2024**, *11*, rbae116.
(50) Lee, S.; Kim, J. H.; Kim, Y. H.; Hong, J.; Kim, W. K.; Jin, S.; Kang, B. J. Sustained BMP-2 delivery via alginate microbeads and polydopamine-coated 3D-Printed PCL/β-TCP scaffold enhances bone regeneration in long bone segmental defects. *J. Orthop. Transl.* **2024**, *49*, 11−22.
(51) Nikhil, A.; Gugjoo, M. B.; Das, A.; Ahmad, S. M.; Kumar, A. 3D-Printed-Cryogel-Impregnated Functionalized Scaffold Augments Bone Regeneration in Critical Tibia Fracture in Goat. *Adv. Healthcare Mater.* **2024**, *13*, 2402619.
(52) Wang, M. J.; Xu, C. F.; Zheng, Y. N.; Pieterse, H.; Sun, Z.; Liu, Y. L. In vivo validation of osteoinductivity and biocompatibility of BMP-2 enriched calcium phosphate cement alongside retrospective description of its clinical adverse events. *Int. J. Implant Dent.* **2024**, *10* (1), 47.
(53) Wei, L. F.; Sun, Y. Y.; Yu, D. D.; Pieterse, H.; Wismeijer, D.; Liu, Y. L.; Wu, Y. Q. The Clinical Efficacy and Safety of ErhBMP-2/BioCaP/β-TCP as a Novel Bone Substitute Using the Tooth-Extraction-Socket-Healing Model: A Proof-of-Concept Randomized Controlled Trial. *J. Clin. Periodontol.* **2025**, *52*, 299.
(54) Akter, K.; Kim, Y.; Choi, E. H.; Han, I. Nonthermal biocompatible plasma in stimulating osteogenic differentiation by targeting p38/ FOXO1 and PI3K/AKT pathways in hBMSCs. *J. Biol. Eng.* **2024**, *18* (1), 35.
(55) Hayashi, K.; Kishida, R.; Tsuchiya, A.; Ishikawa, K. Hematopoietic Function Restoration by Transplanting Bone Marrow Niches In Vivo Engineered Using Carbonate Apatite Honeycomb Bioreactors. *Small Struct.* **2024**, *5* (10), 2400065.
(56) Kapoor, D. U.; Gaur, M.; Kumar, A.; Singh, S.; Chidrawar, V. R.; Prajapati, B. G. Value-added Lignocellulose from Waste Biomass as a Potential Source in Fabrication of Lignin-based Composite for Multifaceted Applications. *Regener. Eng. Transl. Med.* **2024**.
(57) Iervasi, E.; Coronel Vargas, G.; Bachetti, T.; Tkachenko, K.; Spallarossa, A.; Brullo, C.; Rosano, C.; Carta, S.; Barboro, P.; Profumo, A.; et al. A Proteomics Approach Identifies RREB1 as a Crucial Molecular Target of Imidazo-Pyrazole Treatment in SKMEL-28 Melanoma Cells. *Int. J. Mol. Sci.* **2024**, *25* (12), 6760.

https://doi.org/10.1021/acsomega.4c06577
ACS Omega 2025, 10, 10826−10834

(58) Pu, C. Y.; Wang, Y.; Xiang, H. L.; He, J. T.; Sun, Q. Y.; Yong, Y.; Chen, L.; Jiang, K.; Yang, H. F.; Li, Y. L. Zinc-based Polyoxometalate Nanozyme Functionalized Hydrogels for optimizing the Hyperglycemic-Immune Microenvironment to Promote Diabetic Wound Regeneration. *J. Nanobiotechnol.* **2024**, *22* (1), 611.
(59) Liu, Y. H.; Zhu, Z.; Pei, X. B.; Zhang, X.; Cheng, X. T.; Hu, S. S.; Gao, X. M.; Wang, J.; Chen, J. Y.; Wan, Q. B. ZIF-8-Modified Multifunctional Bone-Adhesive Hydrogels Promoting Angiogenesis and Osteogenesis for Bone Regeneration. *ACS Appl. Mater. Interfaces* **2020**, *12* (33), 36978−36995.
(60) Hou, Y. C.; Xu, X. W.; Zhou, Y. Q.; Li, Q.; Zhu, L. L.; Liu, C.; Chen, S.; Pang, J. Versatile Bioactive Glass/Zeolitic Imidazolate Framework-8-Based Skin Scaffolds toward High-Performance Wound Healing. *ACS Appl. Mater. Interfaces* **2024**, *16* (7), 8228−8237.
(61) Kim, M.; Lee, Y. L.; Moon, H. R. Carboxylate-Based Metal-Organic Framework and Coordination Polymer Glasses: Progress and Perspectives. *Acc. Chem. Res.* **2024**, *57* (16), 2347−2357.

https://doi.org/10.1021/acsomega.4c06577
ACS Omega 2025, 10, 10826−10834